Ecological Modelling 220 (2009) 968–978

Contents lists available at ScienceDirect

Ecological Modelling

journal homepage: www.elsevier.com/locate/ecolmodel

Mechanisms of moisture stress in a mid-latitude temperate forest: Implications for feedforward and feedback controls from an irrigation experiment

Justin C. Pettijohn[a,*], Guido D. Salvucci[a,b], Nathan G. Phillips[b], Michael J. Daley[c]

[a] Department of Forest Ecosystems and Society, Oregon State University, 321 Richardson Hall, Corvallis, OR 97331, USA
[b] Department of Geography and Environment, Boston University, 675 Commonwealth Avenue, Boston, MA 02215, USA
[c] Mathematics and Science Department, Lasell College, 1844 Commonwealth Avenue, Newton, MA 02466, USA

ARTICLE INFO

Article history:
Received 14 August 2008
Received in revised form 5 December 2008
Accepted 8 December 2008
Available online 21 February 2009

Keywords:
Transpiration
Stomatal conductance
Moisture stress
Harvard Forest
Red maple (*Acer rubrum* L.)

ABSTRACT

While it is well established that stomata close during moisture stress, strong correlations among environmental (*e.g.*, vapor pressure deficit, soil moisture, air temperature, radiation) and internal (*e.g.*, leaf water potential, sap flow, root-shoot signaling) variables obscure the identification of causal mechanisms from field experiments. Models of stomatal control fitted to field data therefore suffer from ambiguous parameter identification, with multiple acceptable (*i.e.*, nearly optimal) model structures emphasizing different moisture status indicators and different processes. In an effort to minimize these correlations and improve parameter and process identification, we conducted an irrigation experiment on red maples (*Acer rubrum* L.) at Harvard Forest (summers of 2005 and 2006). Control and irrigated trees experienced similar radiative and boundary layer forcings, but different soil moisture status, and thus presumably different diurnal cycles of internal leaf water potential. Measured soil moisture and atmospheric forcing were used to drive a transient tree hydraulic model that incorporated a Jarvis-type leaf conductance in a Penman–Monteith framework with a Cowan-type (resistance and capacitance) tree hydraulic representation. The leaf conductance model included dependence on both leaf matric potential, Ψ_L (so-called feedback control) and on vapor pressure deficit, D (so-called feedforward control). Model parameters were estimated by minimizing the error between predicted and measured sap flow. The whole-tree irrigation treatment had the effect of elevating measured transpiration during summer dry-downs, demonstrating the limiting effect that subsurface resistance may have on transpiration during these times of moisture stress. From the best fitted model, we infer that during dry downs, moisture stress manifests itself in an increase of soil resistance with a resulting decrease in Ψ_L, leading to both feedforward and feedback controls in the control trees, but only feedforward control for the irrigated set. Increases in the sum-of-squares error when individual model components were disabled allow us to reject the following three null hypotheses: (1) the $f(D)$ stress is statistically insignificant ($p = 0.01$); (2) the $f(\Psi_L)$ stress is statistically insignificant ($p = 0.07$); and (3) plant storage capacitance is independent of moisture status ($p = 0.07$).

1. Introduction

Whereas stomatal closure and the subsequent transpiration reduction in response to moisture stress is well documented (Tyree and Sperry, 1989; Sperry and Pockman, 1993; Hubbard et al., 2001; Brodribb and Holbrook, 2003; Larcher, 2003; Sperry, 2003; Vilagrosa et al., 2003), the exact moisture stressing mechanisms in the soil, plant and/or atmosphere are difficult to assess due to the strong correlations among environmental forcing variables of transpiration (*e.g.*, hot and dry, high D, low soil moisture) and internal system status (Ψ_L, depleted stored water, etc.) (Jarvis, 1976a; Franks et al., 1997; Franks, 2004). As such, the development of mechanistically robust models of stomatal response to driving forces, leaf biophysics, and surface energy balance is hampered by the low degree of parameter identifiability, resulting in multiple acceptable (nearly optimal) model structures with different parameter sets and processes (Hornberger and Spear, 1981; Beven, 1993; Beven and Freer, 2001; Werner et al., 2005).

The stomatal conductance of transpiring leaves (g_s) to vapor transport is often modeled using either a Jarvis-type (1976a) or a Ball et al. (1987) formulation (Dewar, 2002). In the Jarvis model, a maximum stomatal conductance ($g_{s,max}$) is reduced through a multiplicative series of stress functions. Typically, three to five stress functions are used in application, representing the sensitivity of stomatal aperture to leaf matric potential (Ψ_L), vapor pressure deficit (D), photosynthetically active radiation (PAR) or

* Corresponding author. Tel.: +1 541 737 9072; fax: +1 541 737 1393.
E-mail addresses: cory.pettijohn@oregonstate.edu (J.C. Pettijohn), gdsalvuc@bu.edu (G.D. Salvucci), nathan@bu.edu (N.G. Phillips), mdaley@Lasell.edu (M.J. Daley).

0304-3800/$ – see front matter © 2008 Elsevier B.V. All rights reserved.
doi:10.1016/j.ecolmodel.2008.12.020

incident shortwave radiation ($S\downarrow$), and air temperature (Stewart and Gay, 1989). While it is relatively straightforward to measure any one stress function at the leaf level (*e.g.*, using a portable leaf-gas exchange system and varying one environmental variable at a time), up-scaling any leaf-level results to ecosystem scales introduces bias due to spatial and temporal variability (Jarvis, 1995). Furthermore, the relative significance of individual stress functions is difficult to assess in whole-tree stand-level studies due to the high degree of correlation among the stressing variables, causing vaguely different parameter sets to yield similar fits to data.

For example, there is debate in the literature about the role of so-called feedforward and feedback responses of stomatal conductance to changes in humidity. In the feedback scenario, increased D raises transpiration and, given the lag in moisture redistribution through the soil–plant continuum to replenish the leaf water and given the increased gradient required to pull water faster through the resistive xylem, the leaf matric potential decreases; stomata may directly sense this increased stress and respond metabolically to affect a reduction in g_s, and/or may close due to reduction in guard cell turgor (Jones, 2007; Eamus et al., 2008). This process can be represented by the Jarvis stress function for Ψ_L. Alternately, the feedforward case involves the stomata responding directly to D, independent of Ψ_L, possibly through differential response of decreased epidermal and guard cell turgor to increased D (Grantz, 1990; Franks et al., 1997; Schroeder et al., 2001). This process can be represented by the Jarvis stress function for D (Macfarlane et al., 2004). Monteith's (1995) analysis of 16 species supports Mott and Parkhurst's (1991) findings that stomata do not directly sense D but close in response to increasing transpiration, lending support to the feedback scenario. Lhomme (2001) uses a one-dimensional soil–plant-atmosphere transfer model to demonstrate that a sole stress function for Ψ_L adequately captures the feedback response of stomata to environmental humidity while a sole stress function for D (independent of Ψ_L), captures feedforward responses. Concurrent to these studies, it has been established that stomata may also respond to direct 'root-to-shoot' communication channel using either abscisic acid (ABA) concentration in the xylem sap or ABA arrival rate to the leaf, further complicating the model representation of g_s (Tardieu and Davies, 1993; Schroeder et al., 2001; Verbeeck et al., 2007).

We conducted an irrigation treatment experiment at Harvard Forest (summers of 2005 and 2006) to investigate feedback and feedforward stomatal regulation of transpiration. We calibrated a non-steady state tree hydraulic model, in which canopy transpiration is estimated using an isothermal Penman (1948)–Monteith (1965) model with a Jarvis (1976a)-type canopy conductance, using scaled heat-dissipation sap flux measurements from both irrigated and non-irrigated sample sets. Ten unknown parameters in the transient model were estimated for 5 sunny days with variable soil moisture and vapor pressure deficit conditions using a hybrid of the modified evolutionary particle swarm optimization algorithm (PSOA), first proposed by Kennedy and Eberhart (1995). While coupled Penman-Monteith and Cowan-type models provide a firm mechanistic basis, they are not alone able to indicate the nature of stomatal feedback or feedforward control. Advances in inverse statistical/numerical parameter estimation techniques (such as the PSOA presented herein) have emerged that can help infer various controls on transpiration using sap flow data.

We tested null hypotheses concerning the significance of the Jarvis moisture stress functions and moisture state-dependence (*i.e.*, Ψ_L) of tissue capacitance by comparing the sum of squared of errors for fully parameterized models with those from models with restricted formulations. Select irrigated (moisture unstressed) and non-irrigated (moisture stressed) red maples (*Acer rubrum* L.) were used in the analysis for 5 select days in 2006. Specifically, we formulated and evaluated the following three null hypotheses: (1) stomatal feedback control is not statistically significant: stomata are insensitive to leaf matric potenial (Ψ_L), (2) stomatal feedforward control is not statistically significant: stomata are insensitive to vapor pressure deficit (D), and (3) tissue capacitance in the dynamic transpiration model is constant and not state-dependent. These three hypotheses were tested using parameter restriction analysis by deactivating either $f(D)$, $f(\Psi_L)$ or the state-dependence of capacitance. In each case, the PSOA was re-run, allowing other model components to potentially compensate for the deactivated term.

2. Theory and experiment

2.1. Whole-tree water flux model

Given that the change rate of xylem water mass (W) (kg) in the transpiring tree can be expressed as

$$\frac{dW}{dt} = J - A_{can}E \tag{1}$$

In Eq. (1), A_{can} is projected canopy area (m^2), E is the transpiration rate per unit area of canopy ($kg\,m^{-2}\,s^{-1}$), and J is the xylem water flow rate ($kg\,s^{-1}$), which can be expressed as the following (Cowan, 1972; Williams et al., 1996):

$$J = \frac{\Psi_S - \Psi_G - \Psi_L}{(R_S + R_P)} \tag{2}$$

In Eq. (2), R_S and R_P are the soil and plant resistances, respectively ($MPa\,s\,kg^{-1}$), Ψ_S is the soil water potential (MPa), Ψ_L is the leaf water potential (MPa), and Ψ_G is the canopy hydrostatic pressure head (MPa), where $\Psi_G = (\rho \cdot g \cdot h_{can}) \cdot 1 \times 10^{-6}$ MPa/Pa, in which ρ the water density ($kg\,m^3$), g is gravitational acceleration ($m\,s^{-2}$), and h_{can} is the canopy height (m). Substitution of Eq. (2) into Eq. (1) yields:

$$\frac{dW}{dt} = \frac{\Psi_S - \Psi_G - \Psi_L}{(R_S + R_P)} - A_{can}E \tag{3}$$

Xylem capacitance (C) ($kg\,MPa^{-1}$) is defined as

$$C \equiv \frac{dW}{d\Psi_L} \tag{4}$$

Next, Eq. (4) is separated and $dW = C \cdot d\Psi_L$ is substituted into the left side of Eq. (3), the result of which is further discretized and separated to yield the following incremental solution for Ψ_L:

$$\Delta\Psi_L = \Delta t \cdot \frac{\Psi_S - \Psi_G - \Psi_L - [A_{can}E(R_S + R_P)]}{C(R_S + R_P)} \tag{5}$$

In Eq. (5), Δt is the model time step (s).

Soil resistance, R_S ($MPa\,s\,kg^{-1}$), can be expressed as the following function of soil hydraulic conductivity (Feddes and Rijtema, 1972; Choudhury and Idso, 1985)

$$R_S = V_s \left[A \cdot \left(\frac{\theta}{n} \right)^c \right]^{-1} \tag{6}$$

In Eq. (6) above, V_s is the estimated root-zone soil volume ($V_s = A_{can} \cdot D_s$, where D_s is the soil depth and is taken as 1 m here), A is a fitting parameter ($kg\,m^3\,MPa^{-1}\,s^{-1}$), θ is the volumetric soil moisture content ($m^3\,m^{-3}$), n is soil porosity ($m^3\,m^{-3}$), and c is taken from the Brooks–Corey relationship as $c = 3 + 2/\lambda_{BC}$. R_P in Eqs. (2)–(5) is the following integrated plant resistance ($MPa\,s\,kg^{-1}$):

$$R_P = r_{p,\text{intrinsic}} \cdot \left(\frac{h_{can} \cdot \chi_1}{A_{xyl}} \right) \tag{7}$$

In the above, $r_{p,\text{intrinsic}}$ ($MPa\,m\,s\,kg^{-1}$) is the intrinsic conductive xylem resistance, χ_1 is a unitless constant accounting for the

influencing of branching effects on the vertical distribution of resistance, and A_{xyl} is conductive xylem cross-sectional area at breast height (m^2). While the R_P is intrinsic for each tree, the loss (and subsequent increase) in conductivity induced by diurnal cavitation (and subsequent repair) is assumed negligible in comparison with the effects of an assumed nonlinear capacitance on measured time lag, as discussed below. Furthermore, as measured Ψ_L magnitudes at Harvard Forest (Bassow, 1995; Williams et al., 1996; Cavender-Bares and Bazzaz, 2000) have not been found to approach cavitation induction levels of approximately −2.5 to −3.0 MPa, the representation of R_P via Eq. (7) was selected, particularly in the assumption of a nonlinear R_S in Eq. (6).

Whereas C in Eqs. (2) and (5) is often assumed to be constant (Williams et al., 1996), recent experiments by Scholz et al. (2007) suggest that there is a nonlinear relationship between midday Ψ_L and C. Furthermore, given recent observed variations in xylem diameter (Sevanto et al., 2006) and the inherent elastic biophysical properties of conductive plant tissue (Goldstein et al., 1998), we assume C is dependent on Ψ_L through:

$$C = A_{xyl} \cdot h_{can} \cdot \chi_2 \cdot c_{\max,\text{intrinsic}} \cdot e^{\alpha \cdot \Psi_L} \tag{8}$$

In the above, χ_2 is a unitless ratio of the true volume of conductive xylem storage volume to that estimated using measured A_{xyl} and h_{can}, $c_{\max,\text{intrinsic}}$ is the intrinsic, unit-volume maximum capacitance ($kg\,MPa^{-1}\,m^{-3}$). Next, α is a unitless shape parameter accounting for non-linear water storage depletion/renewal rates and also non-linear vertical distribution of stored water from the canopy down-stem. As the present model does not have an extra resistance term for the water withdrawn from storage as found in Lhomme et al. (2001), the α shape parameter may account in part for some dynamics attributed to the additional storage resistance.

E ($kg\,m^{-2}\,s^{-1}$) in Eq. (1) is canopy transpiration and is estimated using the isothermal Penman (1948) and Monteith (1965) equation (Raupach, 2001):

$$E = \left(\frac{1}{\lambda}\right) \cdot \frac{\Delta(R_{ni} - G) + \rho_a c_p (g_r + g_h) D}{\Delta + \gamma[(1 + g_r/g_h)/(1 + g_{av}/g_c)]} \tag{9}$$

In Eq. (9), Δ ($Pa\,K^{-1}$) is the slope of the saturation vapor pressure curve, R_{ni} ($W\,m^{-2}$) is the isothermal net available radiation described in Appendix A, G ($W\,m^{-2}$) is the inward heat flux (assumed negligible), ρ_a ($kg\,m^{-3}$) is the air density, c_p ($J\,kg^{-1}\,K^{-1}$) is the isobaric specific heat capacity of air, D (Pa) is the vapor pressure deficit, γ ($Pa\,K^{-1}$) is the psychrometric constant, and g_r ($m\,s^{-1}$) is the following radiative conductance (Raupach, 2001):

$$g_r = \frac{4\varepsilon_s \sigma T_a^3}{\rho_a c_p} \tag{10}$$

In Eq. (10), ε_s is the surface emissivity ($\varepsilon_s = 0.965$ assumed) [unitless], σ is the Stephan–Boltzan constant ($kg\,s^{-3}\,K^{-4}$), and T_a is the air temperature (K); g_h in Eq. (9) is the conductance to sensible heat transport ($m\,s^{-1}$), and is typically assumed equal to the conductivity to vapor transport (g_{av}) which is calculated in a neutral atmosphere as (Brutsaert, 1982):

$$g_{av} = \frac{\kappa^2 U_m}{\ln\,(z_v - z_d/z_{ov}) \ln(z_m - z_d/z_{om})} \tag{11}$$

In Eq. (11), κ is the von Karman constant ($\kappa = 0.41$), U_m is the horizontal wind velocity ($m\,s^{-1}$) at measurement height z_m, z_v is the measurement heights for water vapor transport, z_d is the zero-plane displacement height ($z_d = 0.65 z_{veg}$ is assumed, where z_{veg} is the vegetation height), and z_{om} is the scalar surface roughness length for momentum transport ($z_{om} = 0.1 z_{veg}$ is assumed). z_{ov} in Eq. (11) is the scalar roughness length for water vapor transport, estimated as a fraction, *i.e.*, $kB^{-1}|_v = \ln(z_{om}/z_{ov})$, of z_{om}. Following Brutsaert's (1982) recommendation of an acceptable, first-approximation for practical applications, we have assumed a $kB^{-1}|_v = 2$ (Pettijohn and Salvucci, 2006).

Canopy conductance, g_c ($m\,s^{-1}$) in Eq. (9) was modeled using a Jarvis-type model in which a theoretical maximum stomatal conductance, $g_{s,max}$, is reduced through a multiplicative series of stress functions (Jarvis, 1976b; Jarvis and McNaughton, 1986). In this study, we simplify the Jarvis model to account only for D, Ψ_L, and $S\downarrow$ such that:

$$g_c = g_{s,max} \cdot LAI \cdot f(D) \cdot f(\psi_L) \cdot f(S\downarrow) \tag{12}$$

In Eq. (12), $f(D)$ is a stress function for D. Whereas $f(D)$ is often represented as a linear reduction with a y-intercept equal to one, as proposed by Jarvis (1976a), we formulate $f(D)$ as the following linear branch function, based on our leaf-level measurements, discussed below:

$$f(D) = \left\{ \begin{array}{ll} 1; & 0 \le D \le D_{SS} \\ 1 - \dfrac{D - D_{SS}}{D_{SC} - D_{SS}}; & D_{SS} \le D \le D_{SC} \\ 0; & D \ge D_{SCx} \end{array} \right\} \tag{13}$$

In Eq. (13) above, D_{SS} is the D at which stomatal resistance begins; D_{SC} is a parameter describing the D at which full stomatal closure occurs.

$f(\Psi_L)$ in Eq. (12) is the stress function for leaf matric potential at the mean canopy height; Ψ_L itself is estimated by integrating Eq. (5) forward in time, where the predawn value of Ψ_L is set as: $\Psi_L^{predawn} = \Psi_S^{predawn} - \Psi_G$. Jarvis (1976a) discussed two observed responses of stomatal conductance to Ψ_L: (a) a "linear proportionality" response, *i.e.*, "two sloping straight lines, a threshold region followed by a sloping linear decline," (p. 604), and (b) a continuous curvilinear decline. We utilize the following linear branch function to represent the prior linear proportionality formulation:

$$f(\psi_L) = \left\{ \begin{array}{ll} 1 & ; 0 \le \psi_L \le \psi_{L,SS} \\ 1 - \dfrac{\psi_L - \psi_{L,SS}}{\psi_{L,SC} - \psi_{L,SS}} & ; \psi_{L,SS} \le \psi_L \le \psi_{L,SC} \\ 0 & ; \psi_L \ge \psi_{L,SC} \end{array} \right\} \tag{14}$$

In Eq. (14) above, $\Psi_{L,SS}$ is the Ψ_L at which stomatal resistance begins; $\Psi_{L,SC}$ is a parameter describing the Ψ_L at which full stomatal closure occurs. Canopy height (h_{can}) in Eqs. (2) and (7) was either measured directly using a canopy lift or through allometric equations by Whittaker et al. (1974) from observed relationships between tree height and diameter at breast height (DBH) at the Hubbard Brook experimental forest. Based on our observations of crown geometry using the canopy lift at Harvard Forest, active crown distribution for deciduous species was observed to be distributed in the upper 1/3 of tree height. Furthermore, mean active crown height was assumed to be 2/3 of active crown distribution.

$f(S\downarrow)$ in Eq. (12) is the following stress function for incoming shortwave radiation (Jarvis, 1976a; Stewart and Gay, 1989)

$$f(S\downarrow) = \frac{(1000 + K_2) \cdot S\downarrow}{1000 \cdot (S\downarrow + K_2)} \tag{15}$$

In Eq. (15), K_2 is a constant accounting for the curvature of the stress function.

2.2. Description of study site

The study was conducted during the summers of 2005 and 2006 in the Prospect Hill tract of Harvard Forest, Petersham, MA, United States (42°32′N, 72°10′W, elevation 340 m a.s.l.). Dominant tree species include a mixture of red oak (*Quercus rebura* L.), red maple, black birch (*Betula lenta* L.), paper birch (*Betula papyrifera* L.), eastern hemlock (*Tsuga canadensis* L. *Carrière*) and white pine (*Pinus strobus* L.) (Daley et al., 2007). Red maples were chosen for this irrigation treatment study, as these "super-generalists" naturally grow in a

Table 1
Tree biometry.

Irrigated? (Y/N)	Tree no.	Height[a] (m)	DBH (cm)	Sapwood depth (cm)	Sapwood area (cm^2)	Crown area (m^2)	LAI
Y	1	14.1	14.0	6.2	151.9	8.4	
Y	2	15.1	15.8	6.3	187.2	6.3	4.0
N	4	15.4	16.3	7.1	205.2	16.3	(0.58)
N	5	16.4	18.4	7.2	253.3	21.9	
N	6	14.0	13.8	5.6	145.1	7.9	

[a] Allometric equation used from Whittaker et al. (1974).

wide range of light, moisture and nutrient conditions, contributing to their rapid expansion through North American forests in the twentieth century (Abrams, 1998). Therefore, such responses of this super-generalist may overlap with multiple species and therefore be a good indicator species for temperate forests. Furthermore, our selection of red maple for this study compliments other studies focusing on physiological response to drought stress and/or moisture gradients (Abrams and Kubiske, 1990; Turnbull et al., 2002).

2.3. Irrigation treatment experiment

The irrigation treatment site was located approximately 100 m east of the Little Prospect Hill eddy covariance tower, the proximity of which was situated to best constrain canopy and lower atmospheric boundary layer mass and energy exchanges. A pulse-irrigation system was employed to deliver, on average, approximately 114 l (30 gal) H_2O projected canopy^{-1} day^{-1}, the rate for which was chosen to match the maximum late Spring evapotranspiration rates (~5 mm day^{-1}) measured at the neighboring Little Prospect Hill eddy covariance tower. As projected canopy areas for the irrigated trees were approximately equal to one another (Table 1), irrigation rates were held constant for each irrigated tree. 500 and 1000 gallon self-supporting Rol-la-tank™ relay tanks (WildFire, Alpharette, GA) were situated approximately 100 m uphill from the study area to provide adequate hydraulic head to gravity-drain and thus activate a network of standard soaker garden hoses and/or sprinklers. A programmable multicycle electronic water timer regulated the irrigation system, the cycle lengths for which were determined from early season calibration of average tank drainage rates. As mentioned, root-zone volumetric soil moisture content of the irrigated set of red maples was maintained at early season conditions. However, in the event of a rain event, the irrigation rates were adjusted manually based on observed root-zone θ values following such an event. Once soil dry-downs commenced, the timer program was returned to the normal irrigation routine.

Just as an evaporation pan is designed to measure potential evaporation and, by definition, be small enough not to influence the regional microclimate (Pettijohn and Salvucci, 2009), our select irrigated tree canopies were scattered amongst non-irrigated tree canopies. As such, we assume that our experimental design minimized any anomalously higher vapor concentration in the irrigated canopies due to strong atmospheric mixing.

2.4. Environmental monitoring

2.4.1. Whole tree water flux

Whole tree water flux for the irrigated and reference red maple sets was calculated from estimates of conductive xylem sap velocity profiles inferred from 2 cm heat-dissipation sap flow sensors (Granier, 1987). Sensors were installed principally in the exterior 2 cm of conductive xylem, with select probes installed at conductive xylem depths greater than 2 cm to account for radial variation in sap velocity (Phillips et al., 1996), from which non-dimensional, monotonically decreasing sap velocity profiles were developed. These profiles were then used to convert measured, point-based sap velocities to cross-sectional sap flux in the conductive xylem at measurement height using incremental core data. Finally, stem water flux per xylem cross-sectional area was converted to a unit area canopy energy balance equivalent using projected canopy area measurements found from vertical densitometer measurements. As vertical densiometer estimates of crown area represent the maximum extent of the canopies (by averaging in large canopy gaps), we corrected the projected canopy area measurements on an individual tree basis by normalizing scaled sap flux against eddy covariance water flux during minimally stressed conditions. We isolated the wettest soil conditions over the study period (top 20% volumetric soil moisture content, θ, described below), and normalized the measured transpiration (using the measured canopy area) against the eddy covariance water flux during daytime, clear-sky conditions. While we recognize that red maple represent only one component of the heterogeneous eddy flux footprint, such normalization of the transpiration signals is a critical numerical component in the model parameterization, as the net radiation driving the surface energy balance in the Penman–Monteith transpiration component is assumed to be comparable.

Leaf area index (LAI) of the study area was measured at twenty-one representative locations on August 20, 2006 using an LAI-2000 Plant Canopy Analyzer (LI-COR Environmental, Lincoln, Nebraska, United States). As individual canopies were difficult to isolate from the ground survey locations due to branch overlap from non-sample trees, we utilize the average of these surveys (Table 1) in the model.

2.4.2. Vadose/root-zone moisture conditions

Root-zone θ and temperature profiles for both irrigated and non-irrigated red maple sample sets were monitored at 30-min frequency using Campbell Scientific probes (CS616/CS617 and CS107, respectively). We developed site and depth-specific calibration equations for the TDR probes per Campbell Scientific's recommendations as specified in the CS616 user manual, *i.e.*, *ex situ* θ was determined at various moisture conditions throughout the study period. Further, as the TDR calibration equations are temperature-dependent (particularly at relatively cold conditions), measured soil temperature profiles were applied in the conversion of the TDR raw data (*i.e.*, square wave period) to θ.

Time series of root-zone soil matric potential (Ψ_S) (MPa) profiles were estimated from θ measurements using the following Brooks and Corey (1964) soil water retention curve (SWRC) model:

$$\frac{\theta - \theta_r}{\theta_s - \theta_r} = \left(\frac{\Psi_b}{\Psi_S}\right)^{\lambda_{BC}} \tag{16}$$

In Eq. (16), θ_r is the residual water content ($m^3\ m^{-3}$), θ_s is the saturated water content ($m^3\ m^{-3}$), Ψ_b (MPa) is the air entry soil matric potential, and λ_{BC} is a pore-size distribution index (unitless). *Ex situ* Tempe Cell analyses (SoilMoisture Equipment Corp., Santa Barbara, CA) were conducted on representative soil cores (5.7 cm diameter × 6 cm height) extracted via a SoilMoisture 0200 Soil Core Sampler. Ψ_b, θ_r, and λ_{BC} in Eq. (16) were estimated using a grid search parameterization, in which the root mean squared error (RMSE) was minimized between modeled and measured Ψ_S. Upon

development of the SWRCs for the study area, the measured θ time series is converted to Ψ_S via Eq. (16).

2.4.3. Canopy micrometerology

Canopy micrometeorological conditions (*e.g.*, horizontal wind speed, air temperature, etc.) were measured at the neighboring Little Prospect Hill eddy covariance tower. Additional meteorological variables used in this study, such as incident solar shortwave radiation, were taken from the Fisher meteorological station at Harvard Forest, located approximately 800 m from the primary irrigation site.

2.5. Statistical methods

2.5.1. Parameter estimation

We estimated the ten most unconstrained model parameters, *i.e.*, D_{SS}, D_{SC}, $\Psi_{L,SS}$, $\Psi_{L,SC}$,($c_{\max,\text{intrinsic}}\cdot\chi_2$), ($r_{\text{intrinsic}}\cdot\chi_1$), α, A, K_2, and $g_{s,max}$, using a hybrid particle swarm optimization algorithm (PSOA) as discussed in Pettijohn (2008). The full set of parameters used in the model is shown in Table 2. To maximize the signal to noise ratio and minimize computational time, we isolated 5 'golden days' during the 2006 field season characterized by low cloud cover and a range of comparable and contrasting soil moisture and atmospheric humidity conditions. We then parameterized the transient model for these 5 days using one irrigated and one non-irrigated tree, each of which showed the most significant response to either the irrigation treatment or regional soil moisture stress. The selection of these two trees is discussed in Section 3.1 below.

PSOA is an evolutionary optimization algorithm, in which a population of randomly initialized trial parameter sets (called "particles" in PSOA) dynamically search the parameter space by adjusting individual velocities (*i.e.*, the increment of the parameter dynamic range per search iteration) based on a combination of individual (cognitive) and global (social) historical information about solution behavior (Kennedy and Eberhart, 1995). As such, this metaphorical "swarm intelligence" behavior, manifest in the eventual migration away from local optima and toward the global optimum (*i.e.*, the best solution among all particles), leads to relatively rapid convergence.

A variety of PSOA algorithms have been proposed since being introduced by Kennedy and Eberhart (1995). The most notable differences between algorithms are based on the degree to which particles are either attracted to, or repulsed by, the global optimum, *i.e.*, the best solution of all particles at each iteration (Eberhart et al., 2001). Furthermore, additional behavioral parameters such as particle momentum and random velocity noise have been proposed to increase population 'diversity', *i.e.*, to encourage the exploration of parameter space to avoid premature convergence on local optima. The disadvantage of the more diverse (repulsive) PSOA algorithms is that a prohibitive number of iterations are required for robust performance. To encourage diversity while maintaining rapid convergence, we developed a hybrid PSOA approach by dividing the particle population into the following two groups. We defined two-thirds of the particles in our model using the original attractive PSOA (Kennedy and Eberhart, 1995), while the remaining one-third of the particles followed the "repulsive" PSOA, as described in Eberhart et al. (2001).

The PSOA minimized the following objective function:

$$f(parameters, data) = RSS_{irr} + RSS_{ref} \quad (17)$$

In the above Eq. (17), RSS_{irr} is the residual sum of squares (RSS) for the irrigated tree, RSS_{ref} is the RSS for the non-irrigated tree. Global values for all parameters except $g_{s,max}$ and A were searched upon in the minimization of Eq. (17). We allowed freedom in the parameterization of the $g_{s,max}$ and A parameters for individual trees to minimize projected canopy area measurement errors. In total then, 12 parameters were searched on (8 parameters in common between the two trees, plus two more unique parameters for each tree). In summary, the PSOA was chosen to parameterize the coupled hydraulic model, and therefore distinguish feedback from feed-forward stomatal control, as the PSOA does not require *a priori* assumptions concerning the error structure.

Table 2
Model parameters.

Model parameter	Symbol	Units
Soil resistance fitting parameter	A	kg m^3 MPa^{-1} s^{-1}
Projected canopy area	A_{can}	m^2
Cross-sectional conductive xylem area	A_{xyl}	m^2
Brooks and Corey (1964) parameter	c	–
Conductive xylem capacitance	C	kg MPa^{-1}
Intrinsic, unit-volume maximum capacitance	$c_{\max,\text{intrinsic}}$	kg MPa^{-1} m^{-3}
isobaric specific heat capacity of air	c_p	J kg^{-1} K^{-1}
Vapor pressure deficit	D	Pa
Soil depth	D_s	m
D at which stomatal resistance begins	D_{SS}	Pa
D at which full stomatal closure occurs	D_{SC}	Pa
Canopy transpiration	E	kg m^{-2} s^{-1}
Gravitational acceleration	g	m s^{-2}
Heat flux	G	W m^{-2}
Atmospheric conductance to water vapor transport	g_{av}	m s^{-1}
Canopy conductance	g_c	m s^{-1}
Atmospheric conductance to sensible heat transport	g_h	m s^{-1}
Radiative conductance	g_r	m s^{-1}
Stomatal conductance	g_s	m s^{-1}
Maximum stomatal conductance	$g_{s,max}$	m s^{-1}
Height of canopy	h_{can}	m
Xylem water flux	J	kg s^{-1}
$f(S\downarrow)$ fitting parameter	K_2	–
Soil porosity	n	m^3 m^{-3}
Leaf area index	LAI	m^2 m^{-2}
Total plant resistance	R_P	MPa s kg^{-1}
Isothermal net radiation	R_{ni}	W m^{-2}
Intrinsic conductive xylem resistance	$r_{p,\text{intrinsic}}$	MPa m s kg^{-1}
Total soil resistance	R_S	MPa s kg^{-1}
Incoming shortwave radiation	$S\downarrow$	W m^{-2}
Time	t	s
Horizontal wind velocity at z_m	U_m	m s^{-1}
Root-zone soil volume	V_s	m^3
Xylem water content	W	kg
Zero plane displacement height	z_d	m
Measurement height for U_m	z_m	m
Measurement height for latent heat flux	z_v	m
Vegetation height	z_{veg}	m
Scalar surface roughness length for momentum transport	z_{om}	m
Scalar roughness length for water vapor transport	z_{ov}	m
Capacitance function parameter	α	–
Psychrometric constant	γ	Pa K^{-1}
Slope of saturation vapor pressure curve	Δ	Pa K^{-1}
surface emissivity	ε_s	–
Volumetric soil water content	θ	m^3 m^{-3}
Residual volumetric soil water content	θ_r	m^3 m^{-3}
Saturated volumetric soil water content	θ_s	m^3 m^{-3}
von Karman constant	κ	–
Latent heat of vaporization	λ	J kg^{-1}
Brooks and Corey (1964) pore size distribution index	λ_{BC}	–
Density of water	ρ	kg m^{-3}
Density of air	ρ_a	kg m^{-3}
Stephan–Boltzan constant	σ	kg s^{-3} K^{-4}
Scaling constant in plant resistance function	χ_1	–
Scaling constant in capacitance function	χ_2	–
Air entry soil matric potential	Ψ_b	MPa
Canopy hydrostatic pressure	Ψ_G	MPa
Leaf matric potential	Ψ_L	MPa
Ψ_L at which stomatal resistance begins	$\Psi_{L,SS}$	MPa
Ψ_L at which full stomatal closure occurs	$\Psi_{L,SC}$	MPa
Soil matric potential	Ψ_S	MPa

Table 3
PSOA upper and lower parameter search limits.

Parameter	Lower limit	Upper limit
D_{SS} (Pa)	0×10^{0}	3×10^{3}
D_{SC} (Pa)	1×10^{1}	5×10^{3}
Ψ_{SS} (MPa)	0×10^{0}	3×10^{0}
Ψ_{SC} (MPa)	5×10^{-2}	3×10^{0}
$c_{\max,\text{intrinsic}}$ (kg MPa^{-1} m^{-3})	5×10^{2}	5×10^{3}
$r_{p,\text{intrinsic}}$ (s^{-1})	1×10^{-1}	2×10^{0}
α	1×10^{1}	5×10^{1}
A (MPa^{-1} s^{-1} m^{3} kg)	1×10^{0}	1×10^{2}
χ_{DC}	1×10^{-2}	3×10^{0}
K_2 (W m^{-2})	1×10^{1}	1.5×10^{3}
$g_{s,\max}$ (m s^{-1})	5×10^{-4}	1×10^{5}

2.5.2. Hypothesis formulation and testing using parameter restriction

To test the three null hypotheses presented in the introduction, parameter restriction analysis was performed to assess the statistical significance of changes in the error structure when stress functions 1 ($f(D)$) and 2 ($f(\Psi_L)$) and also the state-dependence of C are deactivated.

The following restricted Jarvis model of g_c was used to test hypothesis 1, *i.e.*, $f(D)$ is insignificant; the feedback $f(\Psi_L)$ stress function alone explain stomatal response to moisture stress:

$$g_c^{X23} = g_{s,\max} \cdot LAI \cdot \ 1 \ \cdot f(\psi_L) \cdot f(S\downarrow) \tag{18}$$

The restricted Penman–Monteith model λE_{PM}^{X23} therefore results from the above restricted canopy conductance g_c^{X23}.

The following restricted Jarvis model of g_c was used to test hypothesis 2, *i.e.*, $f(\Psi_L)$ is insignificant; the feedforward $f(D)$ stress function alone explain stomatal response to moisture stress (if any)

$$g_c^{1X3} = g_{s,\max} \cdot LAI \cdot f(D) \cdot \ 1 \quad f(S\downarrow) \tag{19}$$

The restricted Penman–Monteith model λE_{PM}^{1X3} therefore results from the above restricted canopy conductance g_c^{1X3}.

Finally, to test hypothesis 3, *i.e.*, that tissue capacitance is not state-dependent (non-linear), the restricted Penman–Monteith model λE_{PM}^{CC} was developed, in which a constant value of C is applied in Eq. (1). In other words, in all other transient models but λE_{PM}^{CC}, C is non-linear via the free parameter $\alpha > 0$.

The unrestricted λE_{PM}^{123} model and restricted λE_{PM}^{1X3}, λE_{PM}^{X23} and λE_{PM}^{CC} models were each parameterized by minimizing Eq. (17) using PSOA. Note that in the parameter search, the unrestricted λE_{PM}^{123} model could, with the right choice of parameters D_{SS}, D_{SC}, $\Psi_{L,SS}$, $\Psi_{L,SC}$, fully deactivate the $f(D)$ and $f(\Psi_L)$ stress functions. The unrestricted model is therefore said to encompass the restricted models, an important criteria in applying the statistical tests below.

Table 3 contains the upper and lower limits for the ten unknown model parameters, *i.e.*, D_{SS}, D_{SC}, $\Psi_{L,SS}$, $\Psi_{L,SC}$, $(c_{\max,\text{intrinsic}} \cdot \chi_2)$, $(r_{\text{intrinsic}} \cdot \chi_1)$, α, A, K_2, and $g_{s,max}$, in the PSOA search. The magnitude for each parameter limit corresponds to realistic physical values found either in other studies or in sensitivity analysis conducted prior to the PSOA search.

The null hypotheses were tested by formulating the following test statistic (Pindyck and Rubinfeld, 1998; Wang et al., 2004):

$$\omega = \left(\frac{RSS_r}{RSS_{123}} - 1\right)\frac{T-k}{s} \tag{20}$$

In the above Eq. (20), RSS_r is the restricted model (X23, 1X3 or CRC) RSS, RSS_{123} is the unrestricted model (123) RSS, T is the number of observations used in the PSOA parameterization, k is the number of free parameters in the unrestricted model (*i.e.*, 12), and s is the number of free parameters restricted to zero in the restricted model (*i.e.*, 2 for the X23 and 1X3, representing stress function boundary conditions, and 1 for the CRC, representing α). Next, as ω has been shown to follow the F distribution (Pindyck and Rubinfeld, 1998), a p value associated with the ω can be defined as

$$p = 1 - \int_{-\infty}^{\omega} F_{s,T-k}(x)\ dx \tag{21}$$

In the above Eq. (21), $F_{s,T-k}$ is the F distribution under the null hypothesis. Therefore, the null hypothesis should be rejected at the significance level α when $p < \alpha$.

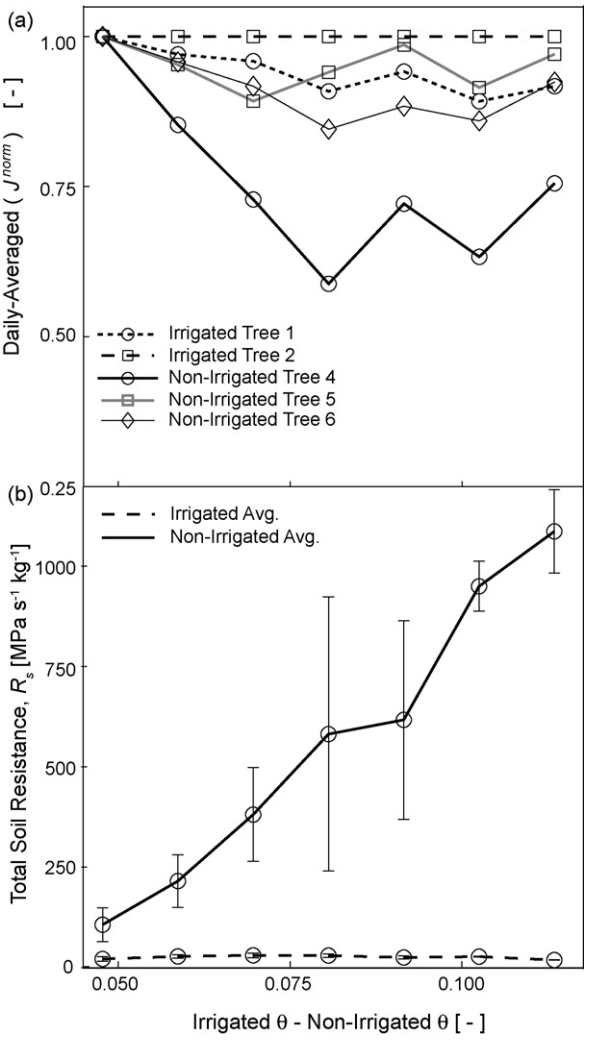

Fig. 1. (a) Individual tree response to regional moisture stress shown as a function of J^{norm} per Eq. (21). Elevated J^{norm} of irrigated red maple treatment set (dashed lines) during regional moisture stress (decreased regional root-zone θ) availability in comparison with decreased, moisture-stressed J^{norm} from non-irrigated maple sample set (solid lines). Non-irrigated tree 5 showed least response to regional moisture stress, possibly due to a deeper rooting depth. (b) Significant increase in non-irrigated (moisture-stressed) R_S during regional dry downs, per Eq. (6).

3. Results and discussion

3.1. Irrigation treatment

As illustrated in Figs. 1a and b and 2a, the irrigation treatment effectively maintained elevated root-zone moisture conditions during regional dry-downs. Fig. 1 x-axis is the difference between the daily averaged irrigated θ and non-irrigated θ and therefore represents regional moisture stress characterizing the non-irrigated trees. The daily averaged J fluxes for each tree in Fig. 1a are

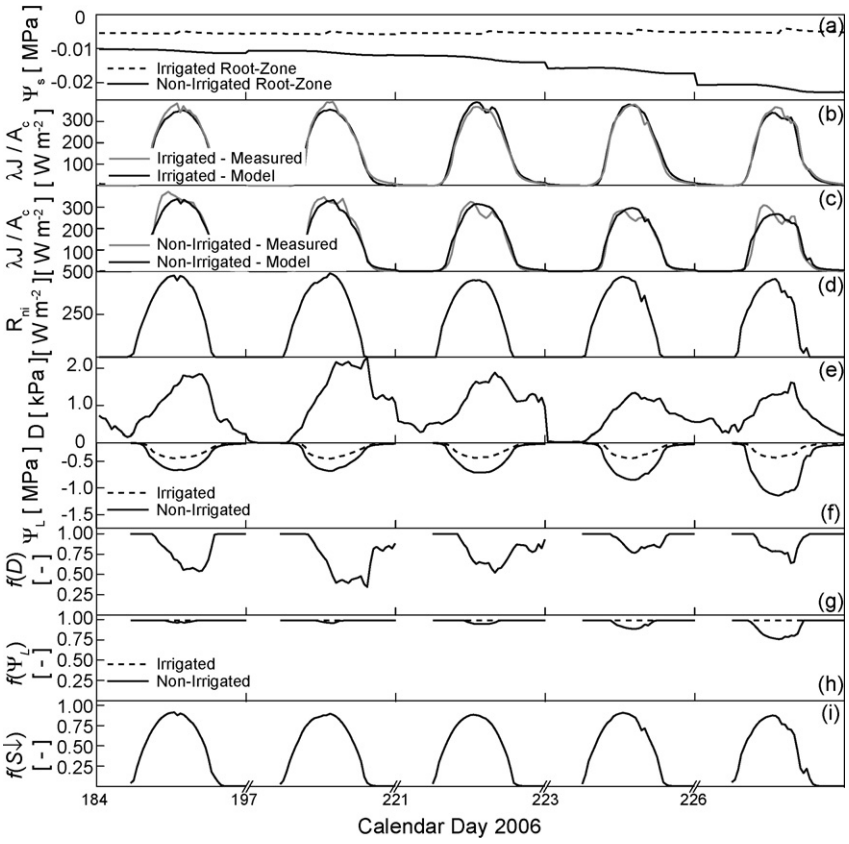

Fig. 2. 2006 dry down time series of: (a) irrigated (dashed) and non-irrigated (solid) root-zone Ψ_S, showing success of irrigation treatment experiment, *i.e.*, irrigated root zones did not experience regional dry down stress; (b) average measured irrigated $\lambda J/A_c$ (small solid line); average of parameterized, unrestricted model of irrigated $\lambda J/A_c$ (bold solid line); (c) average measured non-irrigated $\lambda J/A_c$ (small solid line); average of parameterized, unrestricted model of non-irrigated $\lambda J/A_c$ (bold solid line); (d) modeled R_{ni} used in the isothermal Penman–Monteith canopy transpiration, as described in Appendix A; (e) canopy-level vapor pressure deficit (D) measured from the Little Prospect Hill eddy-covariance tower; (f) average model Ψ_L for irrigated (dashed) and non-irrigated (solid) models; (g) parameterized $f(D)$ stress function in unrestricted models, universal for both irrigated and reference maple sets; (h) parameterized $f(\Psi_L)$ stress function for unrestricted models; equal to unity for irrigated (dashed) while non-irrigated stomata experience Ψ_L stress (solid); (i) $f(S\downarrow)$ stress function.

normalized as

$$J^{norm} = \frac{(J^{bin,i}/J^{bin,1})}{(J^{bin,i}_{irr2}/J^{bin,1}_{irr2})} \tag{22}$$

In Eq. (22) above, $J^{bin,i}$ is the daily averaged J for each tree binned against the x-axis, $J^{bin,1}$ is the "wet" (or first) binned average of daily average J values for each tree, $J^{bin,i}_{irr2}$ is the $J^{bin,i}$ for the second irrigated maple, and $J^{bin,1}_{irr2}$ is the $J^{bin,1}$ for the second irrigated maple.

As seen in Fig. 1a, Irrigated Tree 1 showed less of a response to the irrigation treatment than the Irrigated Tree 2. Next, the non-irrigated Tree 4 showed the most response to the regional dry down, followed by the non-irrigated Tree 6. The non-irrigated Tree 5, however, does not respond as much to regional moisture stress as do the other two non-irrigated trees, probably due to a deeper rooting system with greater access to moisture. We therefore selected the irrigated tree 2 and the non-irrigated tree 4 for use in the parameter estimation, as these trees appear to exhibit the greatest difference in behavior as regional moisture decreases and would therefore highlight feedback and feedforward stress most recognizably.

3.2. Model optimisation—parameter search

3.2.1. Jarvis-type stress function

Parameter values for the unrestricted model found from the proposed hybrid PSOA are shown in Table 4. Fig. 2g through 2i show the relative contributions of the three stress functions during the 2006 dry down. As seen, both $f(D)$ and $f(\Psi_L)$ appear to adequately explain the variance in both irrigated and reference maple sample transpiration sets. Note that $f(D)$ contributes equally in both sets (by construct, $f(D)$ the same for both trees), but $f(\Psi_L)$ only adds significant stress in the non-irrigated reference set because Ψ_L in the irrigated tree never gets low enough to activate $f(\Psi_L)$. This suggests that both sets' stomata have an equal feedforward response $f(D)$ whereas the feedback response $f(\Psi_L)$ is only active in the non-irrigated set. The experimental design, in which all forcing variables are identical on the two trees, but the soil moisture conditions (and thus R_s) vary, yielded enough of a difference in measured sap flux rates for the model to discern feedforward from feedback mechanisms.

The observed decrease in non-irrigated transpiration (Fig. 2c) with increased D lends empirical support to the "overturning" hypothesis (Jones, 1998), *i.e.*, the presence of a threshold E rate with increasing D which cannot be represented merely by a feedback control via Ψ_L. In other words, as the feedback control requires a decrease in Ψ_L, an increase in driving gradient and therefore an increase in E is implied. The addition of a feedforward stress function is, therefore, required to empirically represent this nonlinear "overturning" E–D relationship. While the parameterized Jarvis stress functions for Ψ_L and D are capable, given certain parameter combinations, of reproducing overturning as discussed in Jones (1998), the PSOA parameterized stress functions found herein do not reproduce overturning. We are currently exploring the possibility that Jarvis' product series formulation [see Eq. (12)] may not be flexible enough and that a different function form is required to best represent the elusive stomatal response to D for a given Ψ_L.

Table 4
Parameters from PSOA search for unrestricted (123) and restricted (X23, 1X3, and CRC) models. The average A and $g_{s,max}$ for each model is also included.

Parameter	123	X23	1X3	CRC
D_{SS} (Pa)	811.49	–	704.49	933.14
D_{SC} (Pa)	3063.9	–	3134.0	2974.5
Ψ_{SS} (MPa)	0.6056	0.8727	–	0.6816
Ψ_{SC} (MPa)	2.9373	1.4355	–	1.9282
$c_{max,intrinsic}$ (kg MPa^{-1} m^{-3})	3483.9	1504.3	1038.4	5.2065
$r_{p,intrinsic}$ (s^{-1})	0.6730	1.4504	0.7001	1.0965
α	24.526	21.844	18.327	–
A (MPa^{-1} s^{-1} m^3 kg)	62.767	50.572	64.807	86.604
χ_{DC}	2.9854	0.3767	0.3960	0.9963
K_2 (W m^{-2})	1197.3	1480.7	1161.6	1498.2
$g_{s,max}$ (m s^{-1})	5.3330×10^{-3}	5.0100×10^{-3}	5.2780×10^{-3}	5.4352×10^{-3}
Model performance (N = 480, 30 min data points for combined RM2 and RM4)				
RMSE (W m^{-2})	19.10	28.38	20.28	24.08
r^2	0.9802	0.9566	0.9778	0.9687

As seen in Table 4, a $g_{s,max} = 5.3 \times 10^{-3}$ m s^{-1} was found to best represent the sample sets. Kelliher et al. (1995) compared independent datasets of $g_{s,max}$ for global vegetation, and found an average $g_{s,max} = 6 \times 10^{-3}$ m s^{-1} consistently represents a wide range of datasets, while an average $g_{s,max} = 4.6 \times 10^{-3}$ m s^{-1} $\pm$ 1.7×10^{-3} m s^{-1} was found specific to woody temperate deciduous forests in the dataset. Kelliher et al. (1995) also were careful to note the difference between these leaf-level measurements of $g_{s,max}$ and the model-dependent parameter $g_{s,max}$ in the Jarvis-type relationship, and that measured $g_{s,max}$ were typically found to be 80% of the magnitude of the Jarvis-type $g_{s,max}$. Whereas Turnbull et al. (2002) found no significant difference in $g_{s,max}$ for red maple canopies (conductance at maximum photosynthetic rate at a CO_2 concentration of 36 Pa and saturating PFD, 2000 μmol m^{-2} s^{-1}) along a soil moisture gradient at the Black Rock Forest, New York, their approximate average $g_{s,max} = 4.1 \times 10^{-3}$ m s^{-1} $\pm$ 6.0×10^{-4} m s^{-1} agrees fairly well with our parameterized $g_{s,max} = 5.3 \times 10^{-3}$ m s^{-1}, particularly when taking into account the difference between measured $g_{s,max}$ and that used as a parameter in a Jarvis formulation. It is expected, however, that our allowance of $g_{s,max}$ to be a free parameter results in some absorption in geometric scaling errors associated with *LAI*, projected canopy area and canopy gap fraction measurements.

3.2.2. Whole-tree hydraulic parameters

Plant utilization of water stored in plant tissues can contribute significantly to overall water loss and therefore exert strong hydraulic controls (resistance and capacitance) on transport dynamics inferred from sap flow measurements (Phillips et al., 1997, 2004; Wullschleger et al., 1998; Meinzer et al., 2001, 2003; James et al., 2003; Daley et al., 2008). As such, it is important to couple canopy transpiration models with non-steady state hydraulic models, particularly when inferring canopy level dynamics from lower stem sap flow measurements (Lhomme et al., 2001). As seen in Eq. (2) and, Cowan (1972) used an Ohm's Law R-C circuit analogue to incorporate integrated hydraulic controls such as resistance and capacitance into the whole tree water transport model. These parameters are often experimentally estimated through canopy perturbation and time-series diagnosis (Phillips et al., 1997, 2004; Daley, 2007) or via curvette Schulze et al.'s (1985) or pressure chamber experiments using *ex situ* xylem cores (Meinzer et al., 2003). Whereas capacitance is often modeled using a constant capacitance, *e.g.*, Williams et al. (1996) applied Schulze et al.'s (1985) constant canopy layer capacitance of 8000 mmol MPa^{-1} m^{-2}, the PSOA parameter results of this study indicate that a non-linear, state-dependent capacitance is required to capture the true stored water dynamics that differ throughout the day as stored water from the elastic canopy through the bole xylem is depleted.

As seen in Table 4, a $c_{max,intrinsic} = 3483.9$ kg m^{-3} s^{-1} with corresponding $\alpha = 24.5$ were found to best represent all maples in this study. Typical diurnals of parameterized irrigated and non-irrigated capacitance diurnals are illustrated in Fig. 3, for which the unit volume capacitances have been multiplied by estimated individual tree conductive xylem volume (Table 1). As seen, the parameterized capacitance diurnal in Fig. 3 indicates that there is a time lag in capacitance withdrawal for the irrigated maples. Note that the differences in predawn C between the two trees are forced directly by differences in predawn Ψ_L, initialized each morning to reflect Ψ_S. Of perhaps more significant interest is the essential absence of a capacitance only in the non-irrigated tree from slightly before noon to sunset. As such, a capacitance function has been found that not only explains the morning and evening lags (discharge and recharge of stored water), but also that indicates a lack of time lag from approximately midday onward. It is important to note that, while we assumed that diurnal cavitation and repair (and suqsequent effects of R_P) to be negligible, the parameterized C function may account for such effects on time lag (Phillips et al., 2004). Further, it is important to note that, if we had included an additional storage

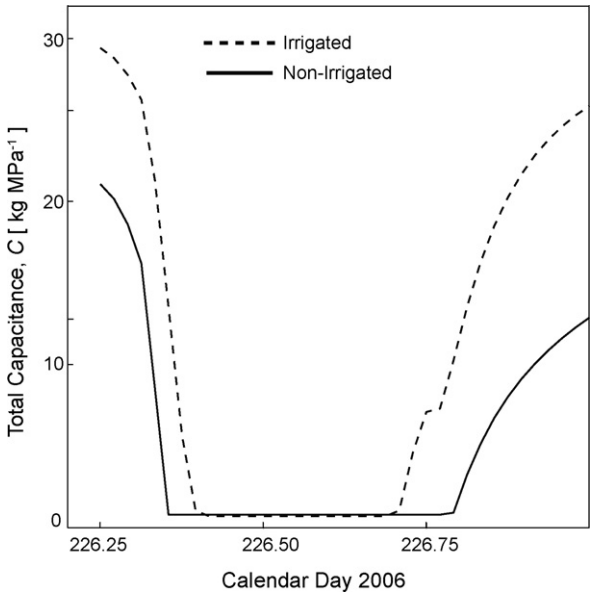

Fig. 3. Parameterized diurnal example of non-linear state-dependent capacitance parameter Eq. (5) using values of $c_{max,intrinsic}$ and α from PSOA shown in Table 4. As seen, greater capacitance is found for the irrigated maple set (heavy dashed line) than for the non-irrigated, moisture-stress maple set (heavy solid line), reflecting greater average transpiration for the irrigated set even though $d\Psi/dt$ is less negative (Ψ less negative for irrigated maples), as shown in Fig. 2f.

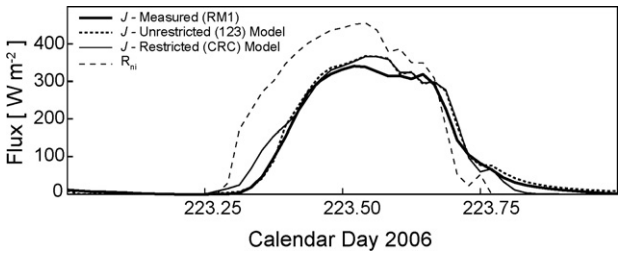

Fig. 4. Demonstration of how the measured morning and evening sap flux time lags (stored water depletion/renewal) for the first irrigated tree, RM1 (solid thick line), are captured in the parameterized unrestricted (123) sap flux (J) RM1 model (short dashed line), in which a moisture state-dependent capacitance is a non-linear function of leaf matric potential (Ψ_L) per Eq. (5). Conversely, the restricted CRC model with constant capacitance is shown (thin solid line) to under-predict stored water utilization (initiate stem sap flux at breast-height too early) and finalize recharge earlier than unrestricted model.

resistance term, as performed by Lhomme et al. (2001), the model optimization would likely have yielded different $c_{max,intrinsic}$ and α values to account for the dynamic interplay of storage resistance and capacitance.

The unrestricted 123 model with the non-linear capacitance per Eq. (8) is compared against the constant capacitance CRC model in Fig. 4. As seen, the non-linearity of the C via Eq. (8) predicts both the morning and evening time lag dynamics more so than the CRC model. It should be noted that the premature rise in J in the CRC model, due to the low constant capacitance, is similarly balanced by a premature decay in J after sunset.

3.3. Subsurface moisture limitations

The time series of Ψ_S, converted from θ using Eq. (16) in the Tempe cell analysis, is shown in Fig. 2a. Ψ_b, θ_r, and λ in Eq. (16), estimated using a grid search method, were found to have values of 20 cm (1 cm), 0 (–), and 0.2803 (0.0169), respectively, with standard deviations indicated in parentheses. Due to the low clay content in these glacially derived stony to sandy loam Typic Dystrochrept soils (Bowden et al., 2004), there is not a large difference in Ψ_s between the irrigated and reference site, even during the largest dry down event (maximum difference of −0.0226 MPa). As such, it cannot be expected that the moisture stress would manifest itself in boundary condition, pre-dawn Ψ_L magnitudes, *i.e.*, a difference in Ψ_L predawn of a few hundredths of an MPa would not have significant effects on λE magnitudes.

The increase in transpiration in response to the irrigation treatment illustrates that this indicator species may be more moisture stressed in dry-downs than might be expected based on plant and soil moisture status, i.e., both the relatively low Ψ_S conditions (due to low clay content and high θ levels) and measured Ψ_L magnitudes (Bassow, 1995; Williams et al., 1996; Cavender-Bares and Bazzaz, 2000) not approaching typical cavitation induction levels (approximately −2.5 to −3.0 MPa). Whereas the transpiration driving gradient ($\Psi_L - \Psi_S$) barely changes as a function of Ψ_S, given the maximum difference of −0.0226 MPa in Ψ_S from the irrigation treatment, and an average Ψ_L = −0.5 to −1 MPa, Ψ_L itself needs to elevate to large (negative) values to overcome the large difference in the approximated R_S Eq. (6), as shown in Fig. 1b, even for a mere 10% reduction in θ. Care should be taken, as red maple rooting depth may be shallower than co-occurring species such as red oak.

3.4. Null hypothesis tests

Table 5 contains ω and p values for the three restricted models. As seen, we can reject the nulls that (1) the $f(D)$ stress function is statistically insignificant at the 1% significance level, (2) that $f(\Psi_L)$ is not significant at the 7% significance level, and (3) that the state-dependence of the capacitance parameter is not significant at the 7% significance level. As seen in Table 4, the RMSEs values of 19.10, 28.38, 20.28 and 24.08 W m^{-2} for the 123, X23, 1X3 and CRC models, respectively, demonstrate the robust performance of all models. The low RMSE differences (and high r^2 values shown in Table 4) between the models demonstrates that parameter indefinability may be seen as advantageous in that many different model representations will perform robustly in minimizing error. It is important to note, however, that the low RMSE differences are statistically significant are therefore allow the identification of parameters representing specific physical mechanisms in the transient tree hydraulic model. The high r^2 values and comparable RMSE magnitudes also reflect the dominance that the diurnal cycles in forcing mechanisms have upon the variance. Close examination of the results of the restricted model, specifically the 1X3 model, shows that without $f(\Psi_L)$, the dry down apparent in Fig. 2c is missed. That is, even though the dry down is an important process, the reduction in RMSE (of approximately 1 W m^{-2} between the 123 and 1X3 models with 20.3 W m^{-2} and 19.1 W m^{-2} RMSE, respectively) due to proper model representation of stress is a small fraction of the errors arising in modeling the diurnal J cycle. In other words, the variance is dominated by diurnal frequencies as opposed to the lower-frequency soil moisture variability signal.

Table 5
Test statistic and significance values used in the hypothesis tests.

Restricted model	ω	p	Reject null?
X23	138.9	0.0072	Yes
1X3	14.70	0.0655	Yes
CRC	135.5	0.0668	Yes

4. Summary and conclusions

The experimental design, in which all forcing variables are identical on the two trees, but the soil moisture conditions (and thus R_s) vary, yielded (1) a significant difference in measured sap flux rates for the model to discern feedforward from feedback mechanisms, and (2) different model Ψ_L magnitudes, and (3) in as much as equifinality is due to strong correlations in Ψ_L and D, the experimental design and subsequent differing Ψ_L magnitudes therefore improves parameter identifiability. We therefore found the feedback response $f(\Psi_L)$ is only active in the non-irrigated set.

Feedback and feedforward controls are difficult to distinguish when parameterizing the model and testing hypotheses using the global dataset, as moderate correlations between maximum daily D and minimum daily non-irrigated Ψ_L (correlation coefficient of −0.3086 for this study period) lead to parameter (mechanistic) indefinability, *i.e.*, the PSOA can choose parameter combination that lead to small objective function differences between model formulations. Furthermore, as D is the driving gradient of transpiration Eq. (9), high D positively correlates with high J via decreases in Ψ_L. Experimental isolation of these correlated forcing mechanisms, as conducted by this irrigation experiment, is therefore required to minimize equifinality and focus on a narrower window of not only optimal, but also mechanistically representative model structures.

In conclusion, our irrigation treatment experiment on red maples (*Acer rubrum* L.) at Harvard Forest (summers 2005 and 2006) allowed us to independently assess feedforward from feedback stomatal control. Our results indicate both feedforward and feedback moisture stress for the non-irrigated trees, with only feedforward controls on the irrigated sample set. Comparison of the restricted and unrestricted models allows us to reject the following three null hypotheses: (1) the $f(D)$ stress function is statistically insignificant at the 1% significance level, (2) the $f(\Psi_L)$ stress function

is not significant at the 7% significance level, and (3) the state-dependence of the capacitance parameter is not significant at the 7% significance level.

Acknowledgments

The authors are grateful to Julian L. Hadley (Harvard Forest, Harvard University), who provided data from the Little Prospect Hill eddy covariance tower at Harvard Forest. Furthermore, the work was conducted with funding from NSF EAR0233643 and NASA LULC Program Grants NAG5-11338 and 11695.

Appendix A. Isothermal net available radiation

R_{ni} in Eq. (9) is the isothermal net available radiation ($W\,m^{-2}$), or the radiation flux density given equal air and leaf temperatures, such that (Gates, 1965, 1966; Paw, 1984):

$$R_{ni} = (1-\alpha_s)(1-e^{-kL})S\downarrow + \varepsilon_s L\downarrow - \sigma\varepsilon_s T_a^4. \quad \text{(A1)}$$

In Eq. (A1), α_s is the surface albedo ($\alpha_s = 0.2$ assumed) and k is the Beer–Lambert light extinction coefficient, calculated at 30-min frequencies as (Campbell and Norman, 1998):

$$k(\psi) = \frac{\sqrt{x^2 + \tan^2(\psi)}}{x + 1.77(x+1.182)^{-0.0733}}. \quad \text{(A2)}$$

In Eq. (A2), ψ is the solar zenith angle and x is the ratio of average projected areas of canopy elements on horizontal and vertical surfaces (Mackay et al., 2003). Further, $L\downarrow$ in Eq. (A1) is the downwelling shortwave radiation ($W\,m^{-2}$), which can be estimated from (Crawford and Duchon, 1999):

$$L\downarrow = [clf + (1-clf)\varepsilon_c]\sigma T_a^4. \quad \text{(A3)}$$

In Eq. (A3), T_a is the air temperature (K) and ε_c is the effective clear-sky atmospheric emissivity, which can be estimated empirically as (Brutsaert, 1975):

$$\varepsilon_c = \left\{ clf + (1-clf)\left[1.24\left(\frac{e_a}{T_a}\right)^{1/7}\right]\right\}. \quad \text{(A4)}$$

In Eq. (A4), e_a is the vapor pressure of the air (mbar), and clf is the cloud fraction, estimated as the difference between modeled $S\downarrow$ to measured $S\downarrow$ (Paltridge and Platt, 1976; Meyers and Dale, 1983; Crawford and Duchon, 1999).

References

Abrams, M.D., 1998. The red maple paradox. Bioscience 48, 355–364.
Abrams, M.D., Kubiske, M.E., 1990. Photosynthesis and water relations during drought in Acer-Rubrum L genotypes from contrasting sites in Central Pennsylvania. Funct. Ecol. 4, 727–733.
Ball, J.T., Woodrow, I.E., Berry, J.A., 1987. A model predicting stomatal conductance and its contribution to the control of photosynthesis under different environmental conditions. In: Biggins, J. (Ed.), Progress in Photosynthesis Research. Martinus Nijhoff Publishers, Dordrecht, pp. 221–224.
Bassow, S.L., 1995. Canopy Photosynthesis and Carbon Cycling in a Deciduous Forest: Implications of Species Composition and Rising Concentrations of CO_2. Harvard University.
Beven, K., 1993. Prophecy, reality and uncertainty in distributed hydrological modeling. Adv. Water Resour. 16, 41–51.
Beven, K., Freer, J., 2001. Equifinality, data assimilation, and uncertainty estimation in mechanistic modelling of complex environmental systems using the GLUE methodology. J. Hydrol. 249, 11–29.
Bowden, R.D., Davidson, E., Savage, K., Arabia, C., Steudler, P., 2004. Chronic nitrogen additions reduce total soil respiration and microbial respiration in temperate forest soils at the Harvard Forest. For. Ecol. Manage. 196, 43–56.
Brodribb, T.J., Holbrook, N.M., 2003. Stomatal closure during leaf dehydration, correlation with other leaf physiological traits. Plant Physiol. 132, 2166–2173.
Brooks, R.H., Corey, A.T., 1964. Hydraulic properties of porous media. Hydrology paper 3. Colorado St. Univ., Fort Collins.
Brutsaert, W., 1975. On a derivable formula for long-wave radiation from clear skies. Water Resour. Res. 11, 742–744.
Brutsaert, W., 1982. Evaporation into the Atmosphere: Theory, History, and Applications. D. Reidel, Hingham, MA, 299 p.
Campbell, G.S., Norman, J.M., 1998. An Introduction to Environmental Biophysics. Springer, New York.
Cavender-Bares, J., Bazzaz, F.A., 2000. Changes in drought response strategies with ontogeny in Quercus rubra: implications for scaling from seedlings to mature trees. Oecologia 124, 8–18.
Choudhury, B.J., Idso, S.B., 1985. An empirical model for stomatal resistance of field-grown wheat. Agric. For. Meteorol. 36, 65–82.
Cowan, I.R., 1972. Oscillations in stomatal conductance and plant functioning associated with stomatal conductance: observations and a model. Planta (Berl.) 106, 185–219.
Crawford, T.M., Duchon, C.E., 1999. An improved parameterization for estimating effective atmospheric emissivity for use in calculating daytime downwelling longwave radiation. J. Appl. Meteorol. 38, 474–480.
Daley, M.J., 2007. Changes in ecohydrological function due to the loss and replacement of eastern hemlock in a New England forest. Ph.D. Dissertation. Boston University, Boston.
Daley, M.J., Phillips, N.G., Pettijohn, C., Hadley, J.L., 2007. Water use by eastern Hemlock (Tsuga canadensis) and black birch (Betula lenta): implications of effects of the hemlock woolly adelgid. Can. J. For. Res. 37, 2031–2040.
Daley, M.J., Phillips, N.G., Pettijohn, J.C., Hadley, J., 2008. Hydraulic responses to environmental perturbations in Tsuga canadensis and Betula lenta. Tree Physiol. 28, 1341–1348.
Dewar, R.C., 2002. The Ball–Berry–Leuning and Tardieu–Davies stomatal models: synthesis and extension within a spatially aggregated picture of guard cell function. Plant Cell Environ. 25, 1383–1398.
Eamus, D., Taylor, D.T., Macinnis-Ng, C.M.O., Shanahan, S., de Silva, L., 2008. Comparing model predictions and experimental data for the response of stomatal conductance and guard cell turgor to manipulations of cuticular conductance, leaf-to-air vapour pressure difference and temperature: feedback mechanims are able to account for all observations. Plant Cell Environ. 31, 269–277.
Eberhart, R., Shi, Y., Kennedy, J., 2001. Swarm Intelligence. Morgan Kauffmann Publishers, San Francisco, p. 550.
Feddes, R.A., Rijtema, P.E., 1972. Water withdrawal by plant roots. J. Hydrol. 17, 33–59.
Franks, P.J., 2004. Stomatal control and hydraulic conductance, with special reference to tall trees. Tree Physiol. 24, 865–878.
Franks, P.J., Cowan, I.R., Farquhar, G.D., 1997. The apparent feedforward response of stomata to air vapour pressure deficit: information revealed by different experimental procedures with two rainforest trees. Plant Cell Environ. 20, 142–145.
Gates, D.M., 1965. Energy, plants, and ecology. Ecology 46, 1–13.
Gates, D.M., 1966. Transpiration and energy exchange. Q. Rev. Biol. 41, 353–364.
Goldstein, G., Andrade, J.L., Meinzer, F.C., Holbrook, N.M., Cavelier, J., Jackson, P., Celis, A., 1998. Stem water storage and diurnal patterns of water use in tropical forest canopy trees. Plant Cell Environ. 21, 397–406.
Granier, A., 1987. Sap flow measurements in Douglas-Fir tree trunks by means of a new thermal method. Ann. Sci. For. 44, 1–14.
Grantz, D.A., 1990. Plant response to atmospheric humidity. Plant Cell Environ. 13, 667–679.
Hornberger, G.M., Spear, R.C., 1981. Approach to the preliminary analysis of environmental systems. J. Environ. Manage. 12 (1), 7–18.
Hubbard, R.M., Ryan, M.G., Stiller, V., Sperry, J.S., 2001. Stomatal conductance and photosynthesis vary linearly with plant hydraulic conductance in ponderosa pine. Plant Cell Environ. 24, 113–121.
James, S.A., Meinzer, F.C., Goldstein, G., Woodruff, D., Jones, T., Restom, T., Mejia, M., Clearwater, M., Campanello, P., 2003. Axial and radial water transport and internal water storage in tropical forest canopy trees. Oecologia 134, 37–45.
Jarvis, P.G., 1976a. The interpretation of the variations in leaf water potential and stomatal conductance found in canopies in the field. Philos. Trans. R. Soc. Lond. Ser. B 273, 593–610.
Jarvis, P.G., 1976b. Interpretation of variations in leaf water potential and stomatal conductance found in canopies in field. Philos. Trans. R. Soc. Lond. Ser. B-Biol. Sci. 273, 593–610.
Jarvis, P.G., 1995. Scaling processes and problems. Plant Cell Environ. 18, 1079–1089.
Jarvis, P.G., McNaughton, K.G., 1986. Stomatal control of transpiration—scaling up from leaf to region. Adv. Ecol. Res. 15, 1–49.
Jones, H., 1998. Stomatal control of photosynthesis and transpiration. J. Exp. Bot. 49, 387–398.
Jones, H.G., 2007. Monitoring plant and soil water status: established and novel methods revisited and their relevance to studies of drought tolerance. J. Exp. Bot. 58, 119–130.
Kelliher, F.M., Leuning, R., Raupach, M.R., Schulze, E.D., 1995. Maximum conductances for evaporation from global vegetation types. Agric. For. Meteorol. 73, 1–16.
Kennedy, J., Eberhart, R., 1995. Particle swarm optimization. In: Neural Networks, 1995. Proceedings, IEEE International Conference on vol. 1944, pp. 1942–1948.
Larcher, W., 2003. Physiological Plant Ecology: Ecophysiology and Stress Physiology of Functional Groups. Springer, Berlin/New York, xx, p. 513.
Lhomme, J.P., 2001. Stomatal control of transpiration: examination of the Jarvis-type representation of canopy resistance in relation to humidity. Water Resour. Res. 37, 689–699.
Lhomme, J.P., Rocheteau, A., Ourcival, J.M., Rambal, S., 2001. Non-steady-state modelling of water transfer in a Mediterranean evergreen canopy. Agric. For. Meteorol. 108, 67–83.

Macfarlane, C., White, D.A., Adams, M.A., 2004. The apparent feed-forward response to vapour pressure deficit of stomata in droughted, field-grown Eucalyptus globulus Labill. Plant Cell Environ. 27, 1268–1280.
Mackay, D.S., Ahl, D.E., Ewers, B.E., Samanta, S., Gower, S.T., Burrows, S.N., 2003. Physiological tradeoffs in the parameterization of a model of canopy transpiration. Adv. Water Resour. 26, 179–194.
Meinzer, F.C., Clearwater, M.J., Goldstein, G., 2001. Water transport in trees: current perspectives, new insights and some controversies. Environ. Exp. Bot. 45, 239–262.
Meinzer, F.C., James, S.A., Goldstein, G., Woodruff, D., 2003. Whole-tree water transport scales with sapwood capacitance in tropical forest canopy trees. Plant Cell Environ. 26, 1147–1155.
Meyers, T.P., Dale, R.F., 1983. Predicting daily insolation with hourly cloud height and coverage. J. Climate Appl. Meteor. 22, 537–545.
Monteith, J.L., 1965. Evaporation and environment. In: Proc. of the 19th Symp. of the Soc. for Experimental Bio. Cambridge University Press, New York, NY, pp. 205–233.
Monteith, J.L., 1995. A reinterpretation of stomatal responses to humidity. Plant Cell Environ. 18, 357–364.
Mott, K.A., Parkhurst, D.F., 1991. Stomatal responses to humidity in air and helox. Plant Cell Environ. 14, 509–515.
Paltridge, G.W., Platt, C.M.R., 1976. Radiative Processes in Meteorology and Climatology. Elsevier, p. 318.
Paw, U.K.T., 1984. A theoretical basis for the leaf equivalence point temperature. Agric. Meteorol. 30, 247–256.
Penman, H.L., 1948. Natural evaporation from open water, bare soil and grass. Philos. Trans. R. Soc. Lond. Ser. A 193, 120–145.
Pettijohn, J.C., 2008. Soil, vegetative and atmospheric controls on the relationship between actual and potential evapotranspiration. Ph.D. Dissertation. Boston University, Boston.
Pettijohn, J.C., Salvucci, G.D., 2006. Impact of an unstressed canopy conductance on the Bouchet–Morton complementary relationship. Water Resour. Res., 42.
Pettijohn, J.C., Salvucci, G.D., 2009. A new two-dimensional physical basis for the complementary relation between terrestrial and pan evaporation. J. Hydrometeorol. 10 (2).
Phillips, N., Oren, R., Zimmermann, R., 1996. Radial patterns of xylem sap flow in non-, diffuse- and ring-porous tree species. Plant Cell Environ. 19, 983–990.
Phillips, N., Nagchaudhuri, A., Oren, R., Katul, G., 1997. Time constant for water transport in loblolly pine trees estimated from time series of evaporative demand and stem sapflow. Trees-Struct. Funct. 11, 412–419.
Phillips, N.G., Oren, R., Licata, J., Linder, S., 2004. Time series diagnosis of tree hydraulic characteristics. Tree Physiol. 24, 879–890.
Pindyck, R.S., Rubinfeld, D.L., 1998. Econometric Models and Economic Forecasts. The McGraw-Hill Companies, New York, xx, p. 634.
Raupach, M.R., 2001. Combination theory and equilibrium evaporation. Q. J. R. Meteorol. Soc. 127, 1149–1181.
Scholz, F.G., Bucci, S.J., Goldstein, G., Meinzer, F.C., Franco, A.C., Miralles-Wilhelm, F., 2007. Biophysical properties and functional significance of stem water storage tissues in Neotropical savanna trees. Plant Cell Environ. 30, 236–248.
Schroeder, J.I., Kwak, J.M., Allen, G.J., 2001. Guard cell abscisic acid signalling and engineering drought hardiness in plants. Nature 410, 327–330.
Schulze, E.D., Cermák, J., Matyssek, M., Penka, M., Zimmermann, R., Vasícek, F., Gries, W., Kucera, J., 1985. Canopy transpiration and water fluxes in the xylem of the trunk of Larix and Picea trees—a comparison of xylem flow, porometer and cuvette measurements. Oecologia 66, 475–483.
Sevanto, S., Holbrook, M., Daley, M.J., Pettijohn, J.C., Phillips, N., 2006. Estimating sap flow using dirunal step diameter variations. In: Harvard Forest Seventeenth Annual Ecology Symposium. Harvard University, Harvard Forest.
Sperry, J.S., 2003. Evolution of water transport and xylem structure. Int. J. Plant Sci. 164, S115–S127.
Sperry, J.S., Pockman, W.T., 1993. Limitation of transpiration by hydraulic conductance and xylem cavitation in Betula-Occidentalis. Plant Cell Environ. 16, 279–287.
Stewart, J.B., Gay, L.W., 1989. Preliminary modelling of transpiration from the FIFE site in Kansas. Agric. For. Meteorol. 48, 305–315.
Tardieu, F., Davies, W.J., 1993. Integration of hydraulic and chemical signaling in the control of stomatal conductance and water status of droughted plants. Plant Cell Environ. 16, 341–349.
Turnbull, M.H., Whitehead, D., Tissue, D.T., Schuster, W.S.F., Brown, K.J., Engel, V.C., Griffin, K.L., 2002. Photosynthetic characteristics in canopies of *Quercus rubra*, *Quercus prinus* and *Acer rubrum* differ in response to soil water availability. Oecologia 130, 515–524.
Tyree, M.T., Sperry, J.S., 1989. Vulnerability of xylem to cavitation and embolism. Annu. Rev. Plant Physiol. Plant Mol. Biol. 40, 19–36.
Verbeeck, H., Steppe, K., Nadezhdina, N., De Beeck, M.O., Deckmyn, G., Meiresonne, L., Lemeur, R., Cermak, J., Ceulemans, R., Janssens, I.A., 2007. Model analysis of the effects of atmospheric drivers on storage water use in Scots pine. Biogeosciences 4, 657–671.
Vilagrosa, A., Bellot, J., Vallejo, V.R., Gil-Pelegrin, E., 2003. Cavitation, stomatal conductance, and leaf dieback in seedlings of two co-occurring Mediterranean shrubs during an intense drought. J. Exp. Bot. 54, 2015–2024.
Wang, J.F., Salvucci, G.D., Bras, R.L., 2004. An extremum principle of evaporation. Water Resour. Res., 40.
Werner, M.G.F., Hunter, N.M., Bates, P.D., 2005. Identifiability of distributed floodplain roughness values in flood extent estimation. J. Hydrol. 314, 139–157.
Whittaker, R., Bormann, F.H., Likens, G.E., Siccama, T.G., 1974. Hubbard Brook ecosystem study—forest biomass and production. Ecol. Monogr. 44, 233–252.
Williams, M., Rastetter, E.B., Fernandes, D.N., Goulden, M.L., Wofsy, S.C., Shaver, G.R., Melillo, J.M., Munger, J.W., Fan, S.-M., Nadelhoffer, K.J., 1996. Modelling the soil–plant-atmosphere continuum in a *Quercus-Acer* stand at Harvard Forest: the regulation of stomatal conductance by light, nitrogen and soil/plant hydraulic properties. Plant Cell Environ. 19, 911–927.
Wullschleger, S.D., Meinzer, F.C., Vertessy, R.A., 1998. A review of whole-plant water use studies in trees. Tree Physiol. 18, 499–512.